Loop punching and bubble rupture causing surface roughening – a model for W fuzz growth

A. Lasa[1], S. K. Tähtinen[1] and K. Nordlund[1]

[1] *Association Euratom-Tekes – Department of Physics, P.O. Box 43, FI-00014 University of Helsinki, Finland*

PACS 52.40.Hf – Plasma-material interactions
PACS 28.52.Fa – Fusion reactor materials
PACS 61.43.Bn – Molecular dynamics calculations and Monte Carlo methods in disordered solids

Abstract – We develop a multi-scale computational for studying tungsten fuzz formation under low-energy He irradiation. The Molecular Dynamics and Kinetic Monte Carlo results show that the W fuzz growth mechanism is the following: the He atoms are trapped in W, forming bubbles and causing growth by loop punching. The bubbles close to the surface rupture. The balance between these processes leads to a stochastic surface growth, causing the surface roughness and fuzz thickness growth to scale as $\sqrt{t}$. The growth rates agree with the experimental results.

Introduction. – ITER aims to be the first TOKAMAK-like fusion reactor producing more energy than it consumes [1]. Its success strongly depends on the appropriate choice of the plasma facing materials (PFMs). Due to its low sputtering yield, low tritium retention, high melting point and high thermal conductivity [2, 3], tungsten (W) is the strongest candidate for the divertor region, where the plasma is designed to touch the wall, leading to extremely intense plasma-wall interactions. On the other hand, helium (He) is produced through the fusion of hydrogen isotopes. W exposed to a He plasma, under the conditions expected for the ITER's reactor, leads to the formation of *fuzz*-like W nano-structures [4]. This surprising effect was not considered in the design of the reactor, making it essential to fully understand the W fuzz growth physics. Extensive experimental effort has been recently put into characterizing the fuzz formation and growth, such as its morphology [5, 6], the effect of fluence [7], flux [8], W-grade [6,9] and plasma temperature [10]. However, the computational or theoretical work is scarce [11, 12], and it explains only qualitatively the experimental findings. The first model in quantitative agreement with the experiments was presented by Martynenko et al. [13], based on the W tendril formation due to the W knock-out (by the incoming He ions) forming adatoms. However, some basic effects of the He irradiation in metals, such as the bubble formation and rupture ([14–17] and references therein) are ignored, which could strongly affect the adatom formation mechanism and overall the surface and tendril morphology.

In the current paper we present a multi-scale model for the W fuzz formation due to low-energy He irradiation. Molecular Dynamics (MD) simulations were used to identify and quantify the basic mechanisms of the W fuzz formation onset and an Object Kinetic Monte Carlo (OKMC) code developed to extend these results to larger length and time scales.

Our multi-scale model shows excellent qualitative and quantitative agreement with the experimental growth rate. The fuzz layer thickness grows with the square root of irradiation time (t), as observed in experiments [7]. According to our model, the driving mechanism is not the He diffusion as initially suggested by Baldwin and Doerner [7], neither the viscoelasticity as proposed by Krasheninnikov [11] nor the stress driven bubble growth as hinted by Sharafat et al. [12], or the knocked-out W adatom formation [13]. Instead, we show that the balance between loop punching and bubble rupture cause the kinetic surface roughening and the consequent fuzz growth to evolve as $\sqrt{t}$.

Methods. – The multi-scale method consisted of two main steps. First, we performed MD simulations of low-energy (60 eV), high flux (10^{27} m^{-2} s^{-1}), high fluence (10^{22} m^{-2}) He and He plus C irradiation on W (100)-surfaces [16], to study the fuzz formation onset and identify the key mechanisms involved in the fuzz growth. The He atoms form bubbles by self-trapping or by trapping to nearby impurities and defects, which induces W loop

punching (i.e. emission of prismatic interstitial dislocation loops due to the high pressure in bubbles [15,18–20]) and consequently surface growth (Fig. 1). If two bubbles grow near to each other, they will coalesce, forming a larger bubble or a network of He bubbles. The bubbles nearest to the surface eventually rupture due to the high He gas pressure, and the surface partially relaxes. The MD simulations show a square root of time dependence of the surface growth − but at a rate orders of magnitude higher than the experimental value, due to the very high flux. These results hint at the loop punching and bubble rupturing as the key processes in the fuzz formation onset and growth. Furthermore, the He reflection yield was quantified (0.4) for a more accurate description of the flux in the OKMC simulations, as described below.

As a second step, we developed a new OKMC code including the following physics insights obtained from the MD study. The OKMC simulations were carried out in a simulation cell with lateral sizes in the range $40-120$ nm. Periodic boundaries were applied in the x and y directions, while the upper z boundary had a 'free' surface that was allowed to develop in height as described below. The lower z boundary was infinitely deep in the simulation, mimicking experimental systems with macroscopic thickness. It is worth noting that no W lattice is explicitly simulated in the OKMC algorithm. The He atoms and bubbles are the objects, and their diffusion, implantation, trapping and clustering, together with the evolution of the W surface (growth and drop) are followed.

In the OKMC algorithm (sketched in Fig. 2), first either a new He atom was implanted − at a random lateral point within the (x-y) size of the simulation cell and at a random depth, following the depth distribution given by SRIM [21]− or an existing single He atom was selected to move, according to the rates dictated by the desired flux and diffusion coefficient ($D = D_0 \cdot e^{E_a/k_B \cdot T}$). The *effective flux* or implantation rate was taken as the desired flux multiplied by 0.6 (1− the He reflection yield). Normal metals, including W, contain $\sim 0.1-1\%$ alloying elements, impurities and/or defects (vacancies, grain boundaries...) that can act as traps for migrating species [22]. To model this effect in the OKMC simulations, the implanted or selected He atom could get trapped with a probability proportional to the trap concentration. If the He is not trapped, it could cluster with a nearby He atom or bubble. After trapping with another He atom [23] or an impurity, the He becomes an immobile bubble that can grow by absorbing additional He atoms within the capture radius of 3 Å (tests showed that the results are not sensitive to the exact value of the trapping radius). In either case, the code looks for bubbles and traps touching each other that would coalesce, followed by checking whether any bubble is closer to the surface than a threshold distance here called *rupture distance*, r_p and given by $r_p = P + M \cdot r$, where r is the bubble radius in Å and $P = 5$ Å, $M = 0.2$ are values estimated from the MD simulations, so that the rupturing distance depends on the bubble size.

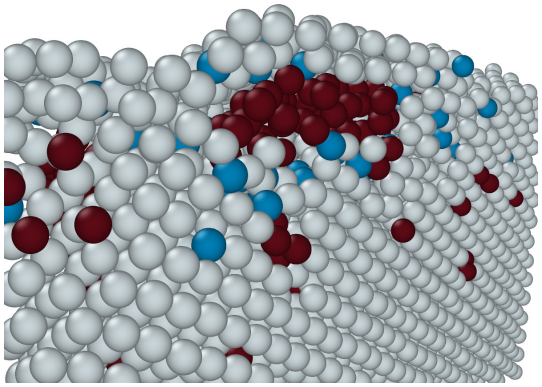

Figure 1: A cross section image, normal to the (110)-plane, of the MD simulation cell [16], after 17000 cumulative He plus C irradiation, showing He trapping around the C-rich region and the loop punching leading to surface growth. The W atoms are coloured in light gray, the He in dark red and C in blue. Ovito was used for visualization purposes [24].

The surface is a 2D cartesian grid with a default size of 60×60 Å and the height of each grid cell varies according to the amount of He beneath it. Finally, the characteristics of the system are analysed, such as the existing and ruptured particle type (He atoms, bubbles, traps), distribution and configuration, surface grid heights, density and fuzz layer thickness. The fuzz is defined as the volume with a density higher than 10% at-W and lower than 90% at-W, based on the experimental results showing a density of 5% at-W [9] and considering that the layers become less and less dense during the irradiation.

Results and Model. –

Results. Running the above described OKMC code under the experimental conditions [7] (effective flux $3{\cdot}10^{22}$, substrate temperature 1120 K, experimental He diffusion coefficient $D_0 = 2.6 \cdot 10^{-4} cm^{-2} s{-}1$ and migration activation energy $E_a = 0.28$ eV [25,26]), we find that the fuzz layer thickness grows following the experimentally measured square root of time dependence (Fig. 3). Given that some characteristics, such as the W-grade, might even double the fuzz growth rate [9], our results are in excellent qualitative and quantitative agreement with the experimental observations.

Next we proceeded to determine the reason for the square root of time dependence. The He diffusion rate in the OKMC simulations was modified by orders of magnitude (including the experimental value given above and the coefficients derived in [7], $D = 6.6 \cdot 10^{-12}$ cm^{-2}s^{-1}, $E = 0.71$ eV). All the different values gave almost identical fuzz thickness growth rates.

We also scanned over a range of trap concentrations ($0.1 - 5\%$) to find its effect and determine the trap con-

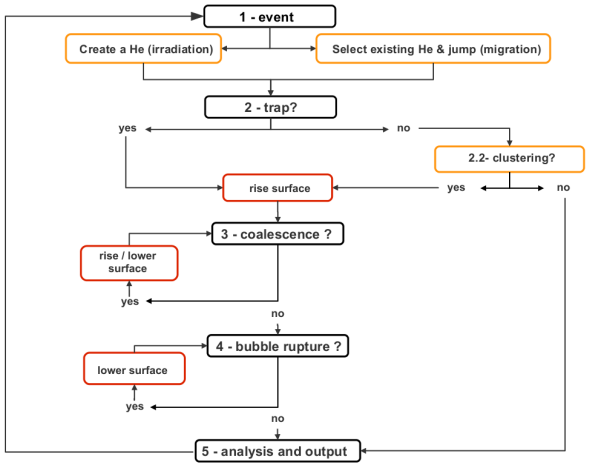

Figure 2: A flowchart of the most important parts of The Object Kinetic Monte Carlo algorithm. The colour coding is as follows: the body of the algorithm (main steps of the sequence) are shown in black. The different options within these steps are coloured in yellow. The surface height modifications are shown in red: rising the height of the surface grid due to trapping, clustering or coalescence where the new particle is located, or lowering it where the coalesed bubbles or ruptured bubbles were. A detailed description of the steps (implantation, diffusion, trapping, the surface rise and lowering, clustering and coalescence) is given in the main text.

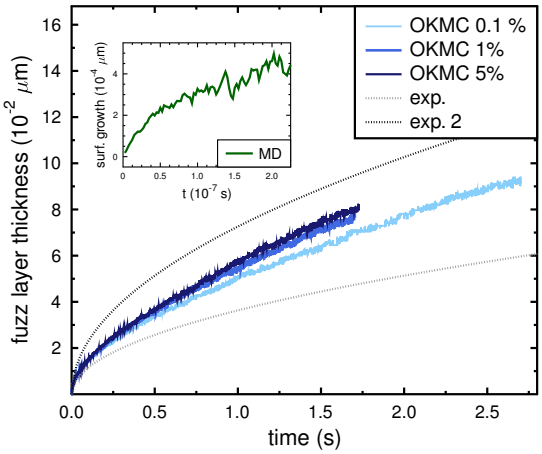

Figure 3: The fuzz layer thickness as a function of time, scanning over different trap concentrations. The experimental data (*exp*) is obtained from the fit of $\sqrt{2Dt}$ to experimental data in Ref. [7]. (*exp.2*) shows a growth twice as fast as (*exp.*), accounting for the possible effect of the W-grade. Note that no parameters fit to the experiments were used in the KMC simulations. Inset: the surface growth of the MD cell as a function of time [16].

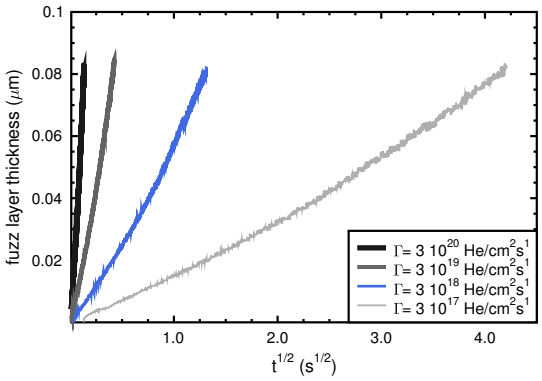

Figure 4: The fuzz layer thickness as a function of the square root of time, scanning over different He fluxes in the OKMC simulations, ranging from $3 \cdot 10^{17} - 3 \cdot 10^{20}$ $\mathrm{m^{-2}s^{-1}}$. The OKMC simulation run using the experimental flux (effectively $3 \cdot 10^{20}$ $\mathrm{m^{-2}s^{-1}}$) is the one compared to the experiments [7] throughout the article.

centration threshold for the fuzz formation (Fig. 3). Even with a low (0.1%) trap concentration, the fuzz thickness grows as $\sqrt{t}$ and a slight increase of the growth rate with the trap concentration is observed, resembling the enhanced fuzz growth found in the experiments using W samples with a large defect content [9].

Further, the present simulations predict a faster fuzz growth as the flux increases (Fig. 4), in qualitative agreement with the experiments [8].

From these scans, together with the MD results showing a surface growth as $\sqrt{t}$ although no diffusion occurs, we conclude that the dominant factor for fuzz growth is the He bubble growth after the He becomes immobile, whereas the He diffusion rate is not relevant for explaining the fuzz growth rate.

Furthermore, the OKMC simulations do not include any lattice stress or viscoelastic effects, nor any W surface diffusion or W knock-out adatom formation, and yet they show the $\sqrt{t}$ dependence, confirming that these mechanisms are not necessary to explain the fuzz growth behaviour. Moreover, the models based on viscoelastic properties [11] or stress driven growth [12] explain only qualitatively the fuzz layer growth, whereas our model allows also a quantitative prediction.

Since the above mentioned mechanisms are ruled out from explaining the fuzz growth rate, we next consider the surface roughness. We found that the surface roughness ($w(t) = \sqrt{\sum_i (z_i(t) - z_{ave}(t))^2}$, where $z_i(t)$ is the height of the surface grid i and $z_{ave}(t)$ is the average surface height at time t) grows as $\sim \sqrt{t}$ (Fig. 5 right). To link the roughness and the fuzz layer growth, we tested setting the same surface height for the whole simulation cell (1×1 grid, a single 60×60 nm W surface, no roughness). In this case, the fuzz layer showed no net growth (Fig. 5

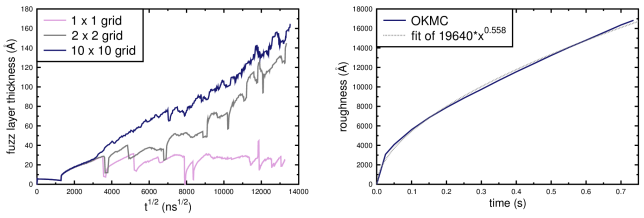

Figure 5: Left: the fuzz layer thickness as a function of the square root of time for a surface divided in a: 1×1 grid (light purple line), 2×2 grid (gray line) and 10×10 grid (dark blue line). Right: the surface roughness *w(t)* of the OKMC simulation cell surface as a function of time (blue solid line) and the fitting to $a \cdot x^b$, with a=0.186 and b=0.558 (gray dashed line) (right).

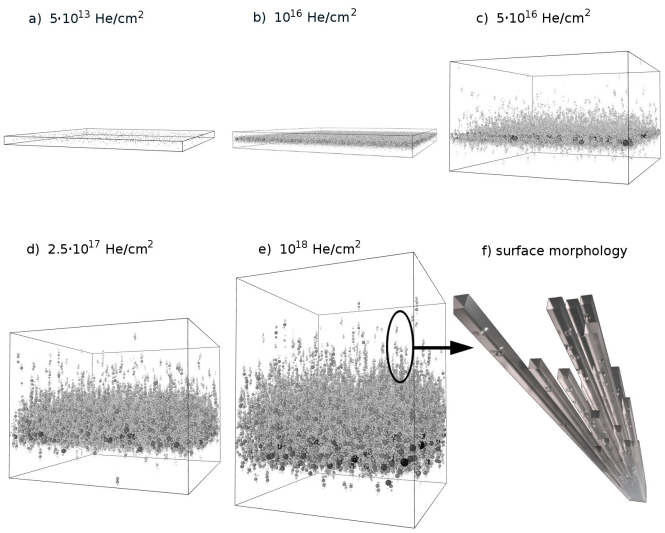

Figure 6: A sequence of 3D snapshots of the OKMC simulation cell, with the surface pointing upwards (the surface grid is not shown here for clarity). a) shows the initial cell (after $5 \cdot 10^{13}$ He/cm^2) with few single He atoms coloured in black. The following figures show the OKMC cell after b) 10^{16}, c) $5 \cdot 10^{16}$, d) $2.5 \cdot 10^{17}$ and e) 10^{18} He/cm^2. The particles are coloured according to their radius, following a gray scale from white (single He atoms) to black (largest bubbles). f) shows a zoom in into one of the surface regions, including the surface grid. In this figure the *glassy* 'material' represents the W beneath the surface and the bubbles are filled with He.

left). By dividing the cell surface into a 2×2 grid (little yet non-negligible roughness), the fuzz layer growth is stepped but almost resembling the square root of time dependence, whereas with a 10×10 grid (a rough surface with with 100 steps of 6×6 nm) the surface evolution is smooth, scales as $\sqrt{t}$ and grows at approximately the experimental rate.

Some other anomalous kinetic roughening processes have been showed to scale as $\sqrt{t}$ too. For example, layer by layer etching of porous films [27], anisotropic plasma etching of composite materials [28] and ion sputtering of polycrystalline solids [29]. All these processes are dominated by a stochastic growth due to the randomly distributed material inhomogeneities (pores, composition or crystal orientation, respectively). The standard deviation for a stochastic growth (or removal) process scales with the square root of the deposited (or removed) mass of material, kinetically evolving as the square root of the fluence or time [30]. We suggest that the $\sqrt{t}$ dependence for the W fuzz growth in He-plasma exposed W is also due to the roughening.

The Model. Considering all the MD and OKMC results described above, we propose the following W fuzz growth model. The He in W forms bubbles by clustering and coalescence. The surface above the bubbles grows by loop punching (Fig. 1). The bubbles will rupture if the the distance to the surface is shorter than the *rupture distance*, r_p. The cell grids, and consequently the fuzz layer, will grow in and outwards, as seen in experiments [9], forming a rough landscape filled with He bubbles, i.e. a porous morphology (Fig. 6). Initially, the surface is smooth and the incoming He is mostly retained, as the surface area for bubble rupturing is a minimum. As the He clusters and the bubbles coalesce, the surface above them grows and becomes rougher. Thus, the area for bubble rupturing increases, lowering the He retention rate and consequently also the fuzz layer growth and surface roughening rates.

Limitations and future work. Although the results from this multi-scale work are in good agreement with the experiments and a consistent physical model for the W fuzz formation and growth is derived, some limitations must be pointed out. The OKMC extended the MD results from ns-Å to μm-second scale, but due to computer capacity limitations, we were unable to reach the experimental hour-mm range. Further, bubble migration is not included in the OKMC code, a process suggested as important in the W fuzz growth [6, 9]. However, due to the strong He self-trapping, the bubble diffusion decays with the number of atoms in the bubble as $1/r^4$ (see Ref. [31] and references therein), reaching a rather negligible migration for medium-sized and large bubbles (> 7 atoms, as a W vacancy is formed) [17]. Hence, considering that the characteristic length scales in the experimental fuzz are in the micron range, bubble migration is unlikely to be the dominant reason for the fuzz growth. Also, the bubbles are spherical in our OKMC code, even when they result from the coalescence of two spherical bubbles, leaving out the *bubble network* found in the MD simulations. However, W fuzz TEM images show that the He bubbles have a rather spherical shape [6].

Also, a systematic modelling study of the experimentally observed fuzz characteristics (e.g., the temperature and irradiation energy thresholds) is needed and ongoing, together with the implementation of the above mentioned missing processes. Further characteristics, such as the ef-

fect of the grain boundaries and different surface orientations could be introduced in our OKMC code if a detailed description of their consequences in the bubble formation, rupture and loop-punching, is provided [17]. Further, the current simulations do not directly address the limited fuzz growth temperature window (approximately $900 - 2000$ K [5,9]). However, the basis of our model are consistent with the following possible explanations.

The trapping of He in impurities, being crucial for the fuzz formation, may explain the upper temperature limit. For a rough estimate, we can take a trap concentration of 0.1%, thus the area per trap is, (atomic area)/(trap concentration) = $10/0.001 = 10000$ Å^2. Considering the experimental flux, $5 \cdot 10^{22}$ m^{-2}s^{-1} the trapping rate is $5 \cdot 10^{22} \times 10000 \cdot 10^{-20} = 5.00 \cdot 10^6$ s^{-1}. On the other hand, at these high temperatures, the He might detrap as well. The He binding energies to different defects (traps) vary with the trapping species, ranging (for the species relevant here) from 0.37 eV for carbon, to 4.57 eV for a vacancy [32]. We take an intermediate value of 2.5 eV and a typical lattice vibration frequency of 10^{13} s^{-1}. Thus, the detrapping rate will be roughly $10^{13} \times e^{(-2.5 \cdot eV/(kB \cdot 2000))} = 5.02 \cdot 10^6$ s^{-1}, which is of the order of the trapping rate. Therefore, at these high temperatures the He will detrap as fast as it is trapped, preventing the cluster formation. Thus, the only cluster nucleation sites will be the larger defects (e.g., grain boundaries and vacancy clusters), leading to fewer and larger bubbles that, when rupturing, cause the experimentally observed pinholes.

The reason for the lower temperature limit is less clear. Experiments show that the morphology feature sizes increase with the temperature [33]. This suggests that the bubble coalescence is more efficient at high temperatures, while at lower ones the He would remain in small nonspherical features. The current KMC implementation cannot simulate this possibility, as it assumes very rapid (faster than the He migration jump time) bubble coalescence, but further development of the simulation algorithm could be used to examine this issue.

I might as well be that the interstitial emission from He traps is thermally activated, meaning that the process would slow down at lower temperatures.

Conclusions. – We conclude that the multi-scale simulation presented here results in very good agreement with experimental findings on W fuzz growth. Atomistic simulations were used to gain insight into the key processes of the W fuzz formation onset and Object Kinetic Monte Carlo simulations to extend these results to longer time and length scales. Based on the multi-scale results we propose a model for the W fuzz growth: 1) The He forms bubbles, which cause surface growth via loop punching. 2) The bubbles located near the surface rupture. 3) The balance between these two processes results in an stochastic surface growth, causing the surface roughness, and consequently the fuzz thickness growth to scale with the square root of time.

* * *

The authors thank Dr. C. Björkas for useful comments on the manuscript, Dr. T. Ahlgren and M. Sc. L. Bukonte for fruitful discussions regarding the He trapping and K.O.E. Henriksson for the assistance in the Molecular Dynamics simulations. This work, supported by the European Communities under the contract of Association between EURATOM/Tekes, was carried out within the framework of the European Fusion Development Agreement (EFDA). The views and opinions expressed herein do not necessarily reflect those of the European Commission. The results of the work were obtained using computational resources of CSC - IT Center for Science Ltd and the Finnish Grid Infrastructure. We acknowledge financial support from the National Graduate School in Materials Physics in Finland.

References

[1] ITER Physics Basis Editors and ITER Physics Expert Group Chairs and Co-Chairs and ITER Joint Central Team and Physics Integration Unit, Nuclear Fusion 39 (1999).

[2] Bolt H., Barabash V., Krauss W., Linke J., Neu R., Suzuki S., Yoshida N. and Team A. U., *Journal of Nuclear Materials*, **329-333, Part A** (2004) 66 proceedings of the 11th International Conference on Fusion Reactor Materials (ICFRM-11).

[3] Roth J., Tsitrone E., Loarer T., Philipps V., Brezinsek S., Loarte A., Counsell G. F., Doerner R. P., Schmid K., Ogorodnikova O. V. and Causey R. A., *Plasma Physics and Controlled Fusion*, **50** (2008) 103001.
http://stacks.iop.org/0741-3335/50/i=10/a=103001

[4] Wright G. M., Brunner D., Baldwin M. J., Doerner R. P., Labombard B., Lipschultz B., Terry J. L. and Whyte D. G., *Nucl. Fusion*, **52** (2012) .

[5] Kajita S., Sakaguchi W., Ohno N., Yoshida N. and Saeki T., *Nuclear Fusion*, **49** (2009) 095005.
http://stacks.iop.org/0029-5515/49/i=9/a=095005

[6] Kajita S., Yoshida N., Yoshihara R., Ohno N. and Yamagiwa M., *J. Nucl. Mater.*, **418** (2011) 152.

[7] Baldwin M. J. and Doerner R. P., *Nuclear Fusion*, **48** (2008) 035001.

[8] Baldwin M., Doerner R., Nishijima D., Tokunaga K. and Ueda Y., *J. Nucl. Mater.*, **390-391** (2009) 886.

[9] Baldwin M. J. and Doerner R. P., *J. Nucl. Mater.*, **404** (2010) 165.

[10] Baldwin M. J., Lynch T. C., Doerner R. P. and Yu J. H., *J. Nucl. Mater.*, **415** (2011) S104.

[11] Krasheninnikov S. I., *Phys. Scr.T*, **145** (2011) 014040.

[12] Sharafat S., Takahashi A., Nagasawa K. and Ghoniem N., *J. Nucl. Mater.*, **389** (2009) 203.

[13] Martynenko Y. and Nagel M., *Plasma Physics Reports*, **38** (2012) 996.
http://dx.doi.org/10.1134/S1063780X12110074

[14] Henriksson K. O. E., Nordlund K., Keinonen J., Sundholm D. and Patzschke M., *Physica ScriptaT*, **108** (2004) 95.

[15] Henriksson K. O. E., Nordlund K. and Keinonen J., *Nucl. Instr. Meth. Phys. Res. B.*, **244** (2006) 377.
[16] Lasa A., Henriksson K. O. E. and Nordlund K., *Nuclear Instruments and Methods in Physics Research Section B: Beam Interactions with Materials and Atoms*, (2012) .
[17] Sefta F., Hammond K. D., Juslin N. and Wirth B. D., *Nuclear Fusion*, **53** (2013) 073015. http://stacks.iop.org/0029-5515/53/i=7/a=073015
[18] Brown L. M. and Woolhouse G. R., *Phil. Mag.*, **21** (1970) 329.
[19] Trinkaus H. and Wolfer W. G., *J. Nucl. Mater.*, **122 & 123** (1984) 552.
[20] Nordlund K., Keinonen J., Ghaly M. and Averback R. S., *Nature*, **398** (1999) 49.
[21] Ziegler J., *The stopping and range of ions in matter* http://www.srim.org/.
[22] Becquart C. S., Domain C., Sarkar U., DeBacker A. and Hou M., *Journal of Nuclear Materials*, **403** (2010) 75.
[23] Henriksson K. O. E., Nordlund K., Krasheninnikov A. and Keinonen J., *Appl. Phys. Lett.*, **87** (2005) 163113.
[24] Stukowski A., *Visualization and analysis of atomistic simulation data with ovito - the open visualization tool* (2010). http://ovito.org/
[25] Amano J. and Seidman D. N., *Journal of Applied Physics*, **56** (1984) 983.
[26] Wagner A. and Seidman D. N., *Phys. Rev. Lett.*, **42** (1979) 515.
[27] Constantoudis V., Christoyianni H., Zakka E. and Gogolides E., *Phys. Rev. E*, **79** (2009) 041604.
[28] Zakka E., Constantoudis V. and Gogolides E., *Plasma Science, IEEE Transactions on*, **35** (2007) 1359.
[29] Marton D. and Fine J., *Thin Solid Films*, **151** (1987) 433 .
[30] Tong W. M. and Williams R. S., *Annual Review of Physical Chemistry*, **45** (1994) 401.
[31] Mikhlin E. Y., *physica status solidi (a)*, **56** (1979) 763. http://dx.doi.org/10.1002/pssa.2210560244
[32] Becquart C. and Domain C., *Journal of Nuclear Materials*, **385** (2009) 223 .
[33] Wright G., Brunner D., Baldwin M., Bystrov K., Doerner R., Labombard B., Lipschultz B., Temmerman G. D., Terry J., Whyte D. and Woller K., *Journal of Nuclear Materials*, **438, Supplement** (2013) S84 .